Dyes and Pigments 81 (2009) 97–102

Contents lists available at ScienceDirect

Dyes and Pigments

journal homepage: www.elsevier.com/locate/dyepig

Quantitative evaluation of solvation and packing effects on the visible absorption of anthraquinone derivatives

Julien Preat*, Denis Jacquemin, Julien Burton, Daniel P. Vercauteren, Eric A. Perpète

Groupe de Chimie Physique Théorique et Structurale, University of Namur (FUNDP), Rue de Bruxelles 61, B-5000 Namur, Belgium

ARTICLE INFO

Article history:
Received 12 September 2008
Accepted 13 September 2008
Available online 1 October 2008

Keywords:
ZINDO
TDDFT
Anthraquinones
Packing effects
Visible spectrum

ABSTRACT

The solvatochromism of five anthraquinone compounds was evaluated at the TD-B3LYP level using the 6-31G(d,p) basis set whilst packing effects were investigated via an approach that combined semi-empirical and ab initio methods, namely ZINDO/TD-B3LYP/6-31G(d,p). This enabled calculation of the colourant's λ_{max} with an average accuracy of 0.14 eV. The packing effects induced large changes in the UV/VIS spectra of the anthraquinones; large bathochromic and hyperchromic displacements were observed.

1. Introduction

Anthraquininoid compounds constitute one of the most popular classes of dyes and pigments, representing ~30% of global colourant production. These compounds owe this popularity due to their abilities to provide a broad range of colours and a capacity to show long wavelength absorption bands. For instance, 9,10-anthraquinone (AQ) **1** (Fig. 1) derivatives can give rise to a large panel of shades, depending on the nature of the side groups. In addition, AQ derivatives also enter the composition of well-known vegetals and can be used to design new drugs. As a consequence, there is an intensive research aiming at designing new AQs, and rationalizing their properties. The organic pigments, especially carbonyls, are in general characterised by larger colour strengths and brightnesses than the inorganic class of pigments, though the former suffer fickle fastness properties [1,2].

The electronic excitation responsible for the colour of anthraquinones is mainly associated to a HOMO–LUMO transition, and presents the π–π^* nature that is typical of conjugated organic molecules. It can be considered that the C=O groups are the active chromophores for which the zwitterionic limiting structures (C^+–O^-) predicted by resonance structure theory have a larger weight in the excited state [3]. The magnitude of the charge separation as well as its stabilisation is directly related to the position and the height of the absorption band. Several factors that would favour a zwitterionic structure can be assessed. For instance, by grafting amino auxochromes in 1,4,5 or 8 positions of AQ, one stabilizes the C^+–O^- form due to hydrogen bonds formation [4]. Apart from these auxochromic effects, the visible spectra of AQ may be strongly affected by the nature of the surroundings of the molecule. In this work, we particularly focused on the solvent (the dielectrical medium stabilizes the excess charge of the carbonyl moeities) and the packing effects (introducing stronger specific intermolecular interactions) on the visible spectra of AQ.

While the methodology used for the evaluation and prediction of the maximum wavelength of absorption (λ_{max}) of AQ dyes in solution is now well established [5–7], there is, to our knowledge, still no consistent procedure designed to evaluate the λ_{max} (in the visible spectrum) of AQ pigments. We have therefore established a supermolecular approach to mimic the model crystal behaviour. The scheme allows to take into account the specific effects due to the intermolecular interactions but suffers important computational costs, which inevitably imply to resort to semi-empirical approaches. Indeed, our supermolecule technique combines the ZINDO [8,9] and the TD-DFT [10–16] schemes to quantify the crystal packing effects on the visible spectra of 1,4-diOH-AQ, 1,4-diNH_2-AQ, 1-NHMe,2-Me-AQ, 1-OH,4-NH(*p*-tolyl)-AQ, and the 1-NH_2,4-NHPh-AQ for which the experimental pigments spectra are available [17]. Difficulties could arise when extrapolating the results obtained from clusters of finite size to the conceptually infinite crystal, although we show that a proper description using 1- D components (constituted by clusters of 2 unit cells) is already sufficient to evaluate semi-quantitatively the packing effects on the λ_{max}.

* Corresponding author.
E-mail address: julien.preat@fundp.ac.be (J. Preat).

0143-7208/$ – see front matter © 2008 Elsevier Ltd. All rights reserved.
doi:10.1016/j.dyepig.2008.09.010

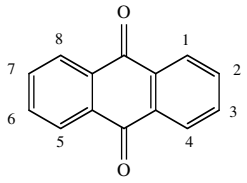

1

Fig. 1. Sketch of the anthraquinone (AQ) and numbering.

2. Computational procedure

All calculations have been performed with the Gaussian 03 [18] suite of programs and the computational scheme is organized in two parts.

2.1. Solvatochromism

In a first step, we evaluate solvatochromism effects by calculating the λ_{max} difference between the isolated and solvated dye. The UV/VIS spectra have been calculated at the TD-B3LYP/6-31G(d,p) level [19,20], which is recognized to be adequate for AQs [5–7]. For the isolated systems, we first perform a so-called gas-phase calculation on the molecules with the experimental crystal geometry whereas, for liquid-phase calculations, the ground state structures of the dyes have been optimized at the DFT/B3LYP level. Following each optimization, the vibrational spectrum has been determined and it has been systematically checked that all vibrational frequencies are real. The bulk solvent effects are taken care off in the TD calculations by using the non-equilibrium Polarizable Continuum Model (PCM) solutions [12,21,22]. In this model, the system is divided into a solute part (the dye) lying inside a cavity, and a solvent part represented as a structureless material and characterised by its dielectric constant as well as other macroscopic parameters. *i*-Propanol is the experimentally used solvent and as the characteristics of this solvent are not available in the standard Gaussian 03 version, we entered the relevant values for the relative dielectric constant, ε_r (EPS = 20.18) as well as the relative dielectric constant at infinite frequency, ε_∞ (EPSINF = 1.896), to stick to the experimental conditions [23].

2.2. Solid-state effects

The evaluation of the pigments λ_{max} follows a two-step methodology:

(1) The crystal structures of the compounds are available in the Cambridge Structural Database (CSD Version 5.28, 11/2006). The ref codes corresponding to 1,4-diOH-AQ; dihydrated 1,4-diNH_2-AQ; 1-NHMe,2-Me-AQ; 1-OH,4-NH(*p*-tolyl)-AQ; and 1-NH_2,4-NHPh-AQ are DHXANT (*Z*, the number of molecules in the unit cell is 4 and the space group is P21/a) [24]; GICXOF (*Z* = 4, *Pnma*) [25]; XAPBIZ (*Z* = 2, P-1) [26]; WISKIS (*Z* = 4, P21) [27]; and FUFDUF (*Z* = 4, P21/c) [28], respectively. For all five systems, the *R* factor is lower than 0.07, ensuring the reliability of the crystallographic structures [29]. As an example, Fig. 2 depicts the orientation of the *a*, *b*, and *c* crystallographic axes for the ($2H_2O$)1,4-diNH_2-AQ and 1,4-diOH-AQ unit cell (UC). Note that most H atoms can generally be located in difference Fourier maps after refinement. The remaining H atoms are calculated geometrically (using the SHELXL97 software [30]) and restrained to ride on their parent atoms.

(2) The evolution of the pigment λ_{max} is provided on the energetic scale (i.e., in eV) by the relation:

$$\lambda_{max}^{pigment}(n,m) = \lambda_{max}^{TD\text{-}DFT}(0,0) \pm \Delta\lambda_{max}^{ZINDO}(n,m) \quad (1)$$

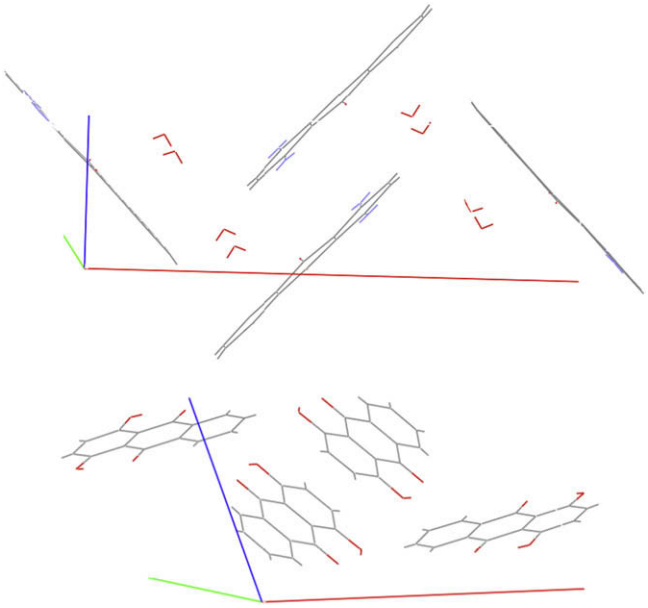

Fig. 2. Crystallographic axes *a* (in red), *b* (in green), and *c* (in blue) associated to the *Pnma* ($2H_2O$) 1,4-diNH_2-AQ (top) and the P21/a 1,4-diOH-AQ (bottom) unit cell. (For interpretation of the references to colour in this figure legend, the reader is referred to the web version of this article.)

In this mixed ab initio/semi-empirical scheme, we calculate the displacement factor (DF) $\Delta\lambda_{max}$ (n,m) of the maximum wavelength of absorption induced by the increase of the cluster size. Because of the large cluster sizes considered, the DF is calculated at the semi-empirical level with ZINDO. The excitation energy of the pigment $\lambda_{max}^{pigment}$ is then obtained by adding the global $\Delta\lambda_{max}^{ZINDO}$ (n,m) to the gas-phase B3LYP λ_{max} (0,0) of the isolated molecule. In Eq. (1), the final sign of $\pm$ is + (−) when the global crystal packing effect is hypsochromic (bathochromic).

The description of 1D packing effects is noted by the growth index GI(*n*) (for a growth of the crystal following the *a* or *b* or *c* axis). More precisely, $n = 0$ corresponds to one isolated molecule, $n = 1$ is associated to one UC and $n = 3$ corresponds then to a 3 UCs cluster. The description of 2D packing effects is noted by the GI(m) (for a growth of the crystal following the *ab* or *ac* or *bc* planes). Note that in the 2D context, $m = 0$ corresponds to one isolated molecule. Fig. 3 illustrates the growth of a crystal following the *b* axis and the *bc* plane; this figure shows that $m = 1$ corresponds to four UCs. For *n* superior or equal to 2, the global packing shift is calculated using:

$$\sqrt{\left(\Delta\lambda_{max}^{ZINDO}(n)\right)_a^2 + \left(\Delta\lambda_{max}^{ZINDO}(n)\right)_b^2 + \left(\Delta\lambda_{max}^{ZINDO}(n)\right)_c^2} \quad (2)$$

whereas for $m \geq 1$, the $\Delta\lambda_{max}^{ZINDO}$ is provided by:

$$\sqrt{\left(\Delta\lambda_{max}^{ZINDO}(m)\right)_{ab}^2 + \left(\Delta\lambda_{max}^{ZINDO}(m)\right)_{bc}^2 + \left(\Delta\lambda_{max}^{ZINDO}(m)\right)_{ac}^2} \quad (3)$$

We provide in Fig. 4 a representation of our procedure: as an example, for a 1D growth of the crystal, the packing effects can be dissociated into three components (three vectors): $(\Delta\lambda_{max}^{ZINDO}(n))_a$, $(\Delta\lambda_{max}^{ZINDO}(n))_b$, $(\Delta\lambda_{max}^{ZINDO}(n))_c$. The resulting vector therefore corresponds to the global packing effects (dotted vector).

3. Results

3.1. Solvatochromism

A characteristic feature of the absorption spectra of numerous AQ derivatives is the existence (in the long wave band) of several

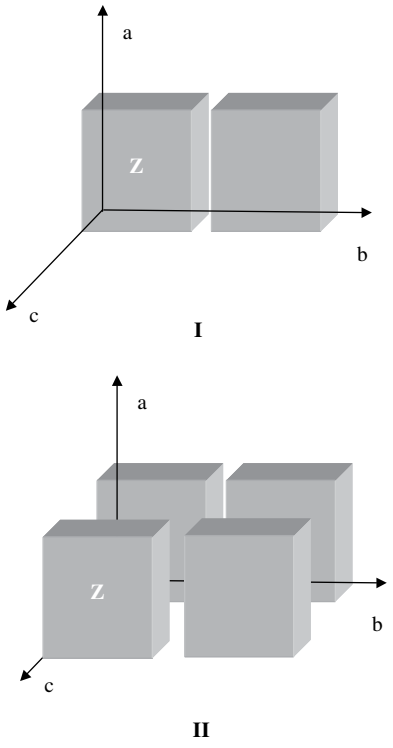

Fig. 3. Illustrative example of a growth of a UC crystal following the *b* axis (up, $n = 1$) and *bc* plane (down, $m = 1$).

maxima resulting from vibrational coupling. That is, the distance between two neighbouring peaks generally sticks to infrared frequencies. As an example, the separation is 1240 cm^{-1} for 1,4-diNH$_2$-AQ and 1160 cm^{-1} for 1-NH$_2$,4-NHPh-AQ. This is close to the typical 1250 cm^{-1} stretching typical of a secondary amino side group. Though, the computation of Franck–Condon factors, which would be required for the full description of such phenomena, lies far outside the scope of the present study.

In Table 1, we compare the λ_{max} calculated in the gas- and liquid-phases. Note that, for all five compounds, the B3LYP/6-31G(d,p) gas-phase geometries provide TD–EEs that are identical to the ones calculated with the X-ray geometries.

Our results indicate that a large dielectric constant proportionally stabilizes the excited states more than it does for the ground state, consequently decreasing (increasing) the EE (λ_{max}). The amplitude of this positive solvatochromism is particularly large for the amino derivatives, whereas for 1,4-diOH-AQ, the dielectric medium has a much smaller impact. As an example, for

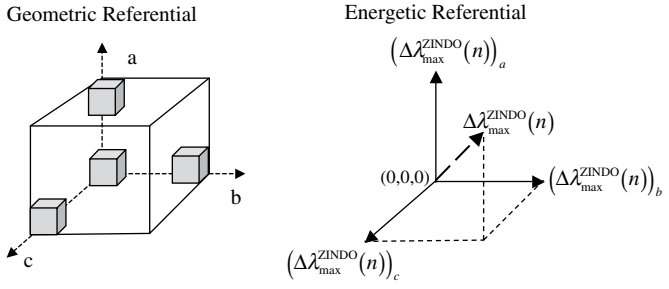

Fig. 4. Illustration of the procedure used for the evaluation of the packing effects: on the right, we depict the growth of the crystal following the three crystallographic axes *a*, *b* and *c* (geometric referential), whereas, on the left, we show the resulting $\Delta\lambda_{max}^{ZINDO}$ displacement of the dye UV/VIS spectrum (energetic referential). In this illustration, $n = 2$ and the (0,0,0) coordinate in the energetic referential corresponds to the $\lambda_{max}^{TD\text{-}B3LYP}(0,0)$.

Table 1
Solvent effects on the visible spectra (λ_{max} of absorption in nm and oscillator strength *f*) of selected five anthraquinone (AQ) derivatives. Liquid-phase calculations have been performed at the PCM-TD-B3LYP/6-31G(d,p)//B3LYP/6-31G(d,p) level of theory. Gas-phase TD-B3LYP/6-31G(d,p) and ZINDO calculations have been performed using the experimental X-ray geometry.

	λ_{max} (*f*)			Exp. [17]
Compounds	TDDFT		ZINDO	
	Isolated	*i*-Propanol		*i*-Propanol
1,4-diOH-AQ	469 (0.17)	471 (0.22)	411 (0.33)	471
1,4-diNH$_2$-AQ	494 (0.18)	539 (0.24)	445 (0.37)	525–554
1-NHMe,2-Me-AQ	485 (0.12)	503 (0.16)	394 (0.27)	503
1-OH,4-NH(*p*-tolyl)-AQ	540 (0.20)	592 (0.28)	445 (0.34)	564–579
1-NH$_2$,4-NHPh-AQ	537 (0.22)	584 (0.31)	458 (0.35)	575–616

1,4-diNH$_2$-AQ, the solvatochromic shift is +45 nm whereas it is only +2 nm for the dihydroxy derivative. For this last compound, we identified a short H bond [–C═O···H–O–] length: 1.66 Å, vs the [–C═O···H–N–] 1.93 Å in 1,4-diNH$_2$-AQ. That is, the H bond induced by grafting hydroxyl groups at positions 1 and 4 on the AQ core is stronger and constitutes the main effect, while the change in the dielectric surroundings can only slightly tune the visible spectrum of 1,4-diOH-AQ. Note that, in 1,4-diNH$_2$-AQ case, the amino auxochrome is planar (i.e., more formally, the NH$_2$ lone pair is delocalized in the AQ core, partly explaining the highest sensitivity of the amino derivatives to the change of the dielectric).

The introduction of the solvent reaction field in the TD scheme leads to a strong hyperchromic shift of the absorption spectrum of all AQs. The increase is 35% in average, the strongest modifications being recorded for 1-OH,4-NH(*p*-tolyl)-AQ and 1-NH$_2$,4-NHPh-AQ with an increase of 40%. This increase of the transition probabilities can be explained as follows: considering the C═O groups as active chromophores, it means that the ground state structure is close to the excited state characteristics (i.e., C^+–O^-).

From the results listed in Table 1, we show that ZINDO systematically overestimates the vertical energies by 97 nm (in average). The gas-phase TD-DFT scheme provides an intermediate MAE (Mean Averaged Error) of 23 nm. The liquid-phase TD-DFT method is more accurate with a MAE of 10 nm. However, we also show that ZINDO predicts auxochromic shifts for the gas-phase λ_{max} (in nm) that are in qualitative agreement with the TD-DFT figures.

3.2. Solid-state effects: dihydroxy and diamino anthraquinones

Table 2 shows the λ_{max}^{ZINDO} evolution for the 1,4-diOH-AQ and 1,4-diNH$_2$-AQ with a 1 dimension (1D) and 2 dimensions (2D) increase of the cluster size.

According to molecular crystal theory, each electronic transition of an isolated molecule in a crystal can be splitted into several excitonic components, i.e., the Davydov splitting [31]. The centre of this resulting excitonic multiplet differs from the excitation energy of the isolated molecule by the packing shift. Therefore, an additional effect (due to the packing shift) in the absorption maximum occurs and the intensities of the bands constituting the multiplet can slightly differ. As an example, we provide in Table 2 two bands of similar oscillator strength constituting a multiplet in the 500 nm (2.5 eV) region of the electromagnetic spectrum (the difference between the two peaks is evaluated to 11 nm/0.05 eV).

For 1,4-diOH-AQ, the variation of λ_{max} with *n* remains equivalent in the three *a*, *b*, and *c* directions, and the 1D packing effects already saturate with $n = 1$. For 1,4-diNH$_2$-AQ UC ($n = 1$), we obtain three λ_{max} with one UC: 473 ($\lambda_{max}(1)$), 461 (λ_{max} (2)), and 447 nm ($\lambda_{max}(3)$) showing a different sensitivity to the cluster size (Table 2). Indeed, the $\lambda_{max}(3)$ does not significantly vary when *n* increases. The second excitation energy is more affected by the growth of the

Table 2
Evolution of the λ_{max}^{ZINDO} (in nm) and f^{ZINDO} vs n for 1D and m for 2D components, n and m being the growth index along the three crystallographic axes a, b, and c, and the planes ab, ac, and bc for 1,4-diOH-AQ and ($2H_2O$) 1,4-diNH_2-AQ. The index $n=0$ corresponds to 1 isolated molecule. For ($2H_2O$) 1,4-diNH_2-AQ, we calculate three λ_{max} with a significant f value. Note that for the 2c system, the $\lambda_{max}(1)$ is splitted into two bands (509 nm and 498 nm) of similar intensity ($f(1)$ of 0.36 and 0.32, respectively).

		1D								2D		
		$n=0$	$n=1$	$n=2$			$n=3$			$m=1$		
				a	b	c	a	b	c	ab	ac	bc
1,4-diOH-AQ	λ_{max}	411	388	388	385	387	389	383	388	385	390	384
	f	0.33	1.11	2.36	1.47	1.35	3.67	1.43	1.29	2.50	2.14	1.93
1,4-diNH_2-AQ	$\lambda_{max}(1)$	445	473	473	470	509 498	474	468	511	477	513	496
	$f(1)$	0.37	0.01	0.16	0.08	0.36 0.32	0.31	0.12	0.48	0.12	0.62	0.65
	$\lambda_{max}(2)$	445	461	469	461	458	469	461	456	468	462	458
	$f(2)$	0.37	0.77	0.62	1.48	0.69	0.99	2.20	0.70	1.24	1.14	1.35
	$\lambda_{max}(3)$	445	447	444	445	450	443	444	452	440	450	447
	$f(3)$	0.37	0.70	1.22	1.36	0.81	1.78	1.99	0.84	2.26	1.44	1.56

crystal whereas, for $\lambda_{max}(1)$ the impact of the packing is not isotropic: the peak position is much more affected by a growth of the crystal following the c axis for which we calculate a (saturated) bathoshift of 66 nm when $n \geq 2$. A molecular orbital analysis coupled to ESP charges (charges fitted to the electrostatic potential) calculations can help to explain the anisotropic behaviour of the 1,4-diNH_2, as well as the weak sensitivity of the $\lambda_{max}(3)$ to the crystal growth:

(1) We depict in Fig. 5 the molecular orbitals (MO) involved in the transition processes, the HOMO-1 and LUMO+3 orbitals [32,33] associated to $\lambda_{max}(1)$ for the 2c ($2H_2O$) 1,4-diNH_2 system (i.e., a growth of the cluster along the c direction with $n=2$). The strong $\lambda_{max}(1)$ bathochromic shift calculated for a growth following the c axis can be interpreted as resulting from the extension of the resonating structure of the LUMO. For $\lambda_{max}(3)$ for which the excitation process mainly corresponds to a transition from the HOMO-2 to the LUMO+1 (Fig. 6), the transition corresponds much more to a pronounced intramolecular charge transfer (CT); the excitation localised on a single molecule of the crystal is almost unsensitive to the crystal packing.
(2) We focus on the ESP atomic charges carried by the neighbouring 1,4-diNH_2-AQ molecules for three clusters corresponding to a growth ($n=2$) of the crystal along the a, b, and c axis. For 1,4-diNH_2-AQ, the PBE0/6-31G(d,p) charges have been evaluated for the dimer (rectangle in Fig. 7) presenting the

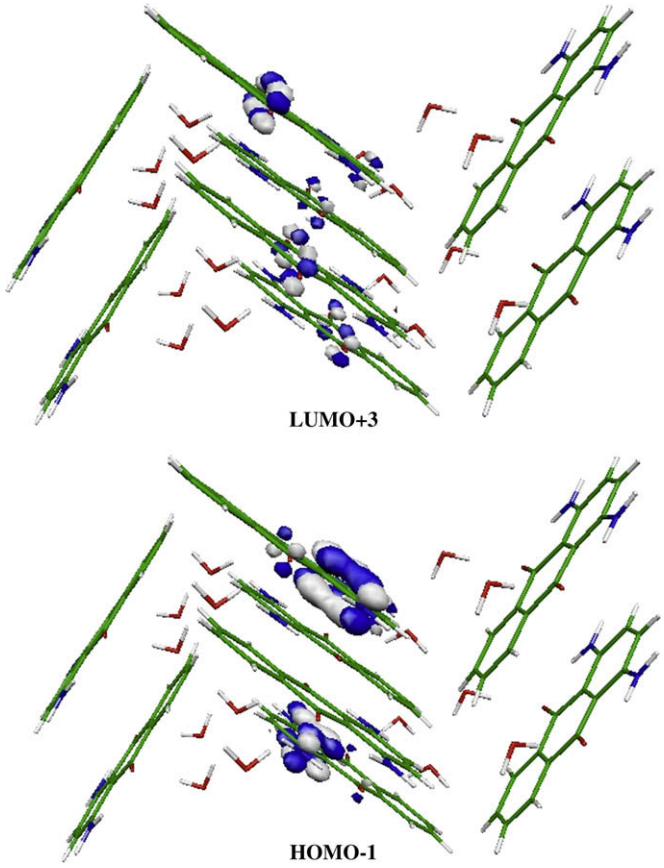

Fig. 5. Active molecular orbitals calculated at the ZINDO level for the $\lambda_{max}(1)$ of 2c ($2H_2O$) 1,4-diNH_2-AQ. The molecular orbitals correspond to isodensity surfaces scaled with the Molekel default values.

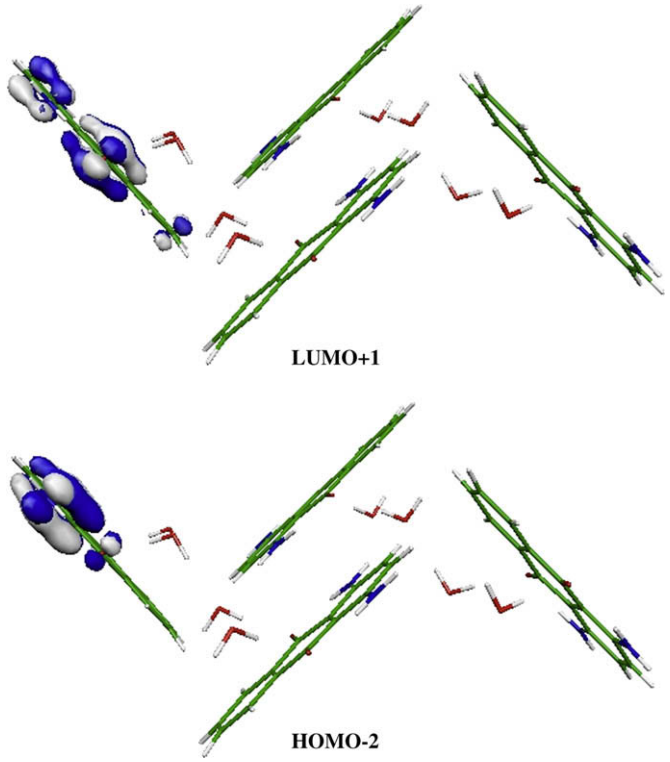

Fig. 6. Active molecular orbitals calculated at the ZINDO level for the $\lambda_{max}(3)$ of 2c ($2H_2O$) 1,4-diNH_2-AQ. The molecular orbitals correspond to isodensity surfaces scaled with the Molekel default values.

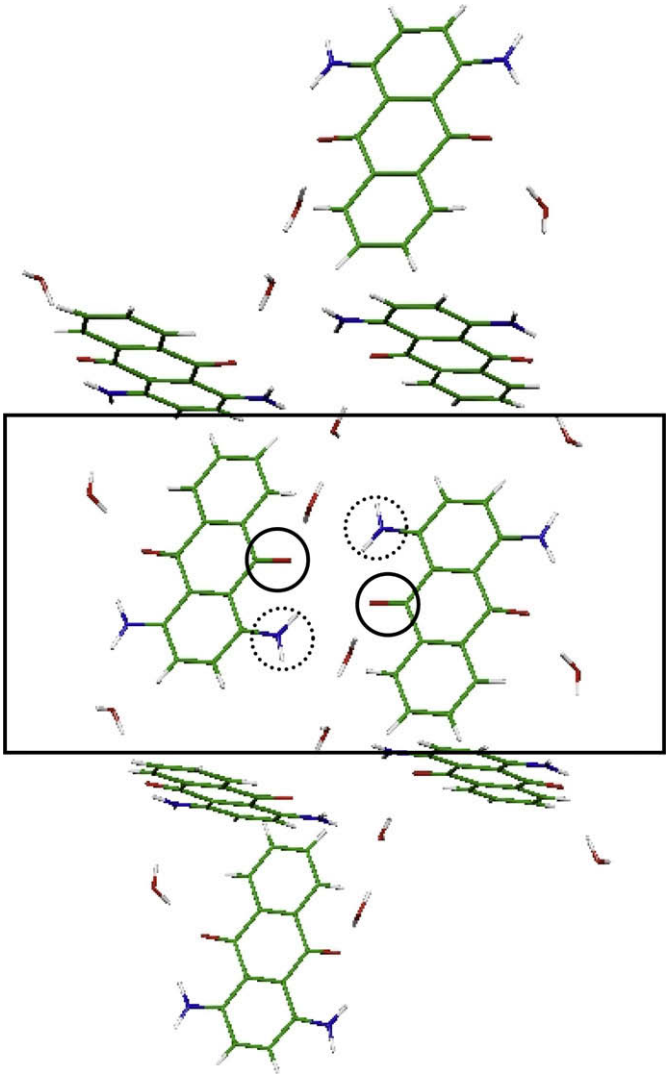

Fig. 7. Schematisation of the ($2H_2O$) 1,4-diNH_2-AQ crystal growth following the *a* axis leading to a 2*a* system, the –NH_2 and the O=C– groups being marked by a dotted and plain circle, respectively.

experimental crystal geometry. More precisely, we calculated an intermolecular –NH_2 (dotted circle) to O=C– (plain circle) distance of 2.54 Å for 2*a* and 2*c*, but much longer for 2*b*, 3.36 Å. The major changes in the ESP charge distribution occur for 2*a* and 2*c* with a decrease of the electronic density on the oxygen atoms; the 2*a* charge distribution is identical to 2*c* and the decrease is 0.043 |e|. Concerning the nitrogen atoms, we record a 0.075 |e| increase of the electronic density. Obviously, the electronic structure of the cluster is more deeply affected by a growth of the crystal following the *a* and *c* axis, explaining in turn the higher sensitivity of the $\lambda_{max}(1)$ and $\lambda_{max}(2)$, for which the intermolecular CT is localised in the region of the crystal where the most important geometrical modifications occur. Since the intramolecular CT coresponding to $\lambda_{max}(3)$ is localised in the region of the crystal where the structure is unaffected by the packing, the transition energy remains constant, whatever the cluster size.

3.3. Visible spectra of the pigments

As several excitation energies were determined for each derivatives, we decided to focus on the most affected λ_{max} by the crystal packing, and owing a sufficiently large oscillator strength (*f*) so that comparisons with respect to experimental data are meaningful. For instance, we focus on the first absorption peak of ($2H_2O$) 1,4-diNH_2-AQ, as this transition is sensitive to the packing and displays large *f* values.

Table 3
Evolution of the λ_{max}^{ZINDO} (in eV) vs *n* for 1D (along the *a*, *b*, and *c* crystallographic axes) and *m* for the 2D components (along the *ab*, *ac*, and *bc* planes) for the five anthraquinones. Note that a zero value of *n* means that only one isolated molecule is considered. It is also important to underline that, because of memory storage limitations, calculations for $n \geq 3$ are not feasible for the 1-OH,4-NH(*p*-tolyl) and the 1-NH_2,4-NHPh derivatives, even at the ZINDO level.

	1D								2D		
	$n=0$	$n=1$	$n=2$			$n=3$			$m=1$		
			a	*b*	*c*	*a*	*b*	*c*	*ab*	*ac*	*bc*
1,4-diOH-AQ	3.02	3.20	3.20	3.22	3.18	3.19	3.23	3.18	3.22	3.18	3.23
1,4-diNH_2-AQ	2.79	2.62	2.62	2.64	2.44	2.61	2.65	2.43	2.60	2.42	2.50
1-NHMe,2-Me-AQ	3.15	3.18	3.20	3.20	3.15	3.22	3.15	3.14	3.23	3.16	3.16
1-OH,4-NH (*p*-tolyl)-AQ	2.79	2.62	2.62	2.60	2.62	–	–	–	2.61	2.62	2.61
1-NH_2,4-NHPh-AQ	2.71	2.63	2.54	2.55	2.56	–	–	–	2.54	2.55	2.55

Table 3 provides the evolution of the five AQ derivatives λ_{max}^{ZINDO}(in eV) with a 1D and 2D increase of the cluster size. In agreement with our previous conclusions (see Section 3.2) the 1D packing effects saturate for $n \geq 2$, i.e., it is not necessary to consider larger clusters for 1D components. Moreover, from the λ_{max} listed in Table 4 for the five studied compounds, we conclude that the 1D description is already satisfactory to evaluate the average packing effects. Indeed, the MAE associated to 1D($n=2$) and 2D($m=1$) are totally similar: 0.15 eV (34 nm) and 0.14 eV (32 nm), respectively. For ($2H_2O$) 1,4-diNH_2-AQ, the packing effects on the λ_{max} are nicely described by the theory, with a slight error of 0.07 eV calculated for the 2D($m=1$) system.

A comparison between the theoretical results listed in Tables 1 and 4 shows that for our five anthraquinones, the packing effects on the UV spectra are much larger than the solvatochromic displacement. For instance, for ($2H_2O$) 1,4-diNH_2-AQ, the packing effects induce a calculated bathochromic shift (2D($m=1$)) of 126 nm, whereas the shift induced by the *i*-propanol (with respect to the gas-phase) is of 45 nm only. Moreover, for four of the studied compounds, our methodology is able to qualitatively reproduce the shift when going from the liquid-phase to the pigment. For instance, for 1,4-diOH-AQ, our methodology delivers a displacement of the absorption band of −53 nm when going from liquid- to the solid-phase (this shift measure is −20 nm). We also show that the theory reproduces the fact that the pigments provide larger colour strengths. Indeed, for ($2H_2O$) 1,4-diNH_2-AQ, we calculate a 43 and 260% increase of the oscillator strength corresponding to the first and second absorption bands.

Table 4
Confrontation between the theoretical [Eqs. (1–3)] and experimental solid-state λ_{max} in eV (in nm) for the five anthraquinones. Theoretical values are provided for a 1D and 2D growth of the crystal along the three crystallographic axes *a*, *b*, and *c* and the planes *ab*, *ac*, and *bc*. The experimental λ_{max} correspond to *n* or $m=\infty$. The index $n=0$ corresponds to one isolated molecule [$\lambda_{max}^{TD\text{-}B3LYP}(0,0)$].

	1D			2D	Exp. [17]
	$n=0$	$n=1$	$n=2$	$m=1$	*n* or $m=\infty$
1,4-diOH-AQ	2.64 (469)	2.95 (420)	2.95 (420)	2.97 (418)	2.75 (451)
1,4-diNH_2-AQ	2.51 (494)	2.34 (530)	2.09 (593)	2.00 (620)	1.98 (627)
1-NHMe,2-Me-AQ	2.56 (485)	2.59 (480)	2.63 (471)	2.64 (470)	2.38 (520)
1-OH,4-NH(*p*-tolyl)-AQ	2.30 (540)	2.13 (582)	1.99 (623)	2.15 (576)	2.05 (606)
1-NH_2,4-NHPh-AQ	2.31 (537)	2.23 (556)	2.03 (611)	2.03 (611)	1.91 (650)

4. Conclusions

We have established a mixed ZINDO–TD-DFT three-step procedure to evaluate the absorption spectrum of five anthraquinone crystals with a precision of +/− 0.17 eV or +/− 35 nm.

In our methodology, the packing effects have been decomposed into three components: the three crystallographic axes *a*, *b*, and *c* (1 dimension growth), on the one hand, and the three plans *ab*, *ac*, *bc* (2 dimension growth), on the other hand. Since the mean averaged error, from the test set of five target molecules, associated to the 1D and 2D models are equivalent, we deduced that only a 1D description of the components is satisfactory to evaluate the average packing effects. We also have demonstrated that, for the set of studied anthraquinoic systems, the packing effects on the UV/VIS spectrum are more important than solvatochromism. As an outlook, we are currently extending this study to other classes of dyes. Moreover, since the excitation energies in the solid-state show strong charge transfer (CT) characters, the description of such excited states should be sensitively improved by including long-range (LR) effects in the model. More precisely, one of the problems that hybrid functionals encounter is the underestimation of the energy of charge transfer electronic transitions. This DFT limitation has for origin the shortsightedness of functionals, i.e., the erroneous asymptotic behaviour of the exchange potential. One of the strategies to correct this "wrong" behaviour is to use an optimized effective potential for exact exchange that explicitly considers the LR effects. This scheme leads to the range-separated hybrids that use a growing fraction of exact exchange when the interelectronic distance increases [34,35].

Acknowledgments

J.P. thanks the F.N.R.S. for his grant as "Collaborateur Scientifique". J.B. acknowledge the Belgian F.R.I.A. for his PhD grants. D.J. and E.A.P. thank the Belgian F.N.R.S. for their research associate positions. The calculations have been performed on the Interuniversity Scientific Computing Facility (ISCF), installed at the FUNDP (Namur, Belgium), for which the authors gratefully acknowledge the financial support of the FNRS-FRFC and the "Loterie Nationale" for the convention number 2.4578.02. The authors thank Catherine Michaux for her valuable advices and help.

References

[1] Christie RM. Colour chemistry. Cambridge: Royal Society of Chemistry; 2001.
[2] Perkins AG, Everest AE. The natural organic coloring matters. London: Longmans; 1918.
[3] Jacquemin D, Preat J, Charlot M, Wathelet V, André JM, Perpète EA. J Chem Phys 2004;121:1736.
[4] Jacquemin D, Preat J, Wathelet V, André JM, Perpète EA. Chem Phys Lett 2005;405:429.
[5] Perpète EA, Wathelet V, Preat J, Lambert C, Jacquemin D. J Chem Theor Comput 2006;2:434.
[6] Jacquemin D, Assfeld X, Preat J, Perpète EA. Mol Phys 2007;105:325.
[7] Savko M, Kascakova S, Gbur P, Miskovsky P, Ulicny J. J Mol Struct (THEOCHEM) 2007;823:73.
[8] Zerner MC, Iowe GH, Kirchner RF, Mueller-Westerhoff UT. J Am Chem Soc 1980;102:589.
[9] Zerner MC. Rev Comp Chem 1991;2:313.
[10] Guillaumont D, Nakamura S. Dyes Pigments 2000;46:85.
[11] Adamo C, Barone V. Chem Phys Lett 2000;330:152.
[12] Cossi M, Barone V. J Chem Phys 2001;115:4708.
[13] Baerends EJ, Ricciardi G, Rosa A, van Gisbergen SJA. Coord Chem Rev 2002;230:5.
[14] Wilberg KB, de Oliveria AE, Trucks G. J Phys Chem A 2002;106:4192.
[15] Preat J, Jacquemin D, Wathelet V, André J-M, Perpète EA. J Phys Chem A 2006;110:8144.
[16] Jacquemin D, Preat J, Wathelet V, Fontaine M, Perpète EA. J Am Chem Soc 2006;128:2072.
[17] Yatsenko AV, Chernyshev VV, Popov SI, Sonneveld EJ, Schenk H. Dyes Pigments 2000;45:169.
[18] Frisch MJ, Trucks GW, Schlegel HB, Scuseria GB, Robb Ma, Cheeseman JR, et al. GAUSSIAN 03, revision B. 04. Pittsburg, PA: Gaussian Inc.; 2003.
[19] Lee C, Yang W, Parr RG. Phys Rev B 1988;37:785.
[20] Becke AD. J Chem Phys 1993;98:5648.
[21] Amovilli C, Barone V, Cammi R, Cancès E, Cossi M, Mennucci B, et al. Adv Quantum Chem 1998;32:227.
[22] Tomasi J, Mennucci B, Cammi R. Chem Rev 2005;105:2999.
[23] Available from: http//www.Sigmaaldrich.com/catalog/ProductDetail/ALDRICH/278475, Copyright 2007, Sigma-Aldrich Co, 2007.
[24] Nigam GD, Deppisch B. Z Kristallogr 1980;151:185.
[25] Kashino S, Senoo K, Haisa M. Acta Crystallogr C 1988;44:104.
[26] Yatsenko AV, Paseshnichenko KA, Popov SI. Z Kristallogr 2000;215:542.
[27] Yatsenko AV, Zhukov SG, Medvedev SV, Stalnaya TV. Acta Crystallogr C 1996; 52:55.
[28] Kurucsev T, Snow MR, Tiekink ERT. Acta Crystallogr C 1987;43:2226.
[29] Krebs FC. J Appl Crystallogr 2000;33:392.
[30] Sheldrick GM. SHELXL97. Germany: University of Göttingen; 1997.
[31] Lisitsa MP, Kharchenko NP. J Appl Spectrosc 1968;8:405.
[32] Portmann S, Lüthi HP. Chimia 2000;54:766.
[33] Flükiger P, Lüthi HP, Portmann S, Weber J. MOLEKEL 4.3. Manno, Switzerland: Swiss Center for Scientific Computing; 2002.
[34] Heyd J, Scuseria GE, Ernzerhof M. J Chem Phys 2003;118:8207.
[35] Jacquemin D, Perpète EA, E Scuseria G, Ciofini I, Adamo C. J Chem Theor Comput 2008;4:123.